ISSN 0386-5878
Technical Memorandum
of PWRI No. 2790

Model Test on Avalanche Energy Dissipator (Part 1)

July, 1989

SLOPE FAILURE DIVISION
EROSION CONTROL DEPARTMENT
PUBLIC WORKS RESEARCH INSTITUTE
MINISTRY OF CONSTRUCTION

1-Asahi, Tsukuba city, Ibaraki Prefecture, 305 JAPAN

Technical Memorandum
of PWRI No. 2790

Model Test on Avalanche Energy Dissipator (Part 1)

Slope Failure Division

Hiroyuki Yoshimatu

Kazunori Fujisawa

Jiro Oura

Niigata Experimental Laboratory

Chuichi Shimomura

Hideki Terada

Synopsis:

Avalanche Control Facilities are broadly grouped into Avalanche Prevention Facilities which are constructed in potential avalanche areas to prevent avalanches, and facilities for protection from avalanches by either stopping them, changing their course or dissipating them.

Of the latter facilities, avalanche energy dissipators which stop avalanches before some object to be protected, by dissipating the velocity of the avalanche, are not yet fully understood in terms of their effects and design.

This study was conducted for steel structures to be used as energy dissipators in order to determine the impact of an avalanche crashing against the avalanche dissipator and to define the dissipation effect by the avalanche dissipator.

Two kinds of tests, one using parlite as an avalanche material and the other using artificial snow produced by ice slicers, were conducted to compare the avalanche impact and the dissipation effect between these two materials.

The results were able to express the impact of the parlite and the artificial snow against the piles of the energy dissipator used in this study, through an equation for fluid impact. With respect to the blocking effect, these two materials showed different results. The bouncing angle of the parlite and the artificial snow that crashed against one lateral pile was approximately 40 degrees (against the horizontal direction downstream the slope), while the impact against the second row pile, when two lateral piles were used, was very minor compared with that against the first row pile. The dissipation effect of the energy dissipator was given by the difference between the impulse of the avalanche impact in the absence of the energy dissipator, and the avalanche impact in the presence of the energy dissipator.

In a test using artificial snow and energy dissipator piles arranged in a triangle form consisting of two perpendicular piles in the first row and one perpendicular pile in the second row, the avalanche flow which was narrowed due to the first row pile was received by the second row pile, and so the impact on the second row pile was greater than that on the first row pile in many cases.

A comparison among the dissipation effects of various model dissipators using the artificial snow showed that a jungle gym triangle model was the most effective.

Key Words: Avalanche, Avalanche Energy Dissipator

PREFARENCE

This booklet is translated from the original technical memorandum of

P.W.R.I. No. 2468

CONTENTS

1. Outline of Tests

1.1. Test by Parlite

The test equipment largely consists of a running down slope, a flow induction wall, a failure box and a retaining wall. The acryl flow induction walls are placed on both sides of the running down slope and are 30 cm wide. The failure box is placed on the top edge of the slope, and parlite (water content of 50%, 0.1 m^3, 25 kg) filled in the failure box and made to run down the slope by opening the front door of the failure box. Various dissipator piles are set on the downstream of the slope. In addition, the retaining wall is placed on the lowest end of the slope. (Figure 1)

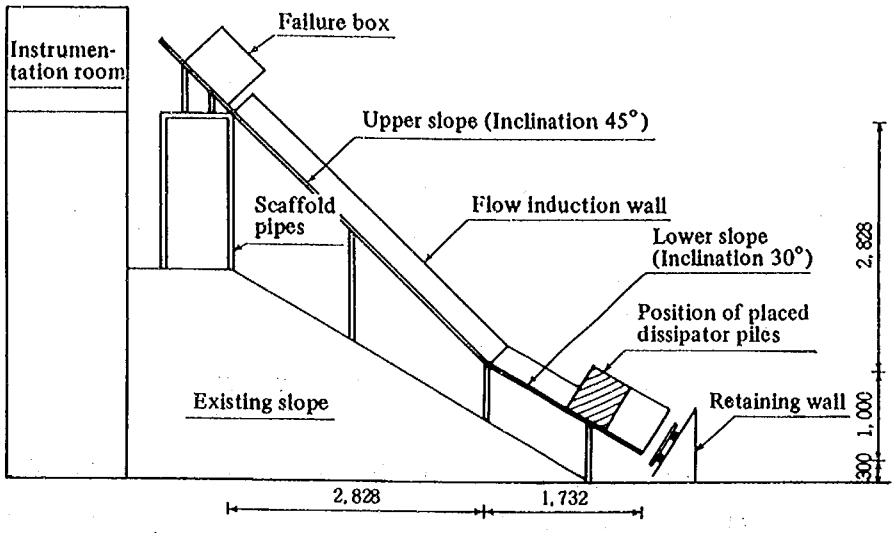

Figure 1. Outline of parlite test

A test starts when the front door of the failure box is opened on the "ready" sign and the parlite is allowed to run down naturally. The impact exerted on the dissipator pile by the moving parlite is determined by a load cell placed on the pile. The parlite smashes against the dissipator pile and flies away to change its course, and finally collide against the retaining wall placed on the lowest edge of the slope. The parlite, after collision, stops and is deposited downstream. The impact of the parlite at the time of collision on the retaining wall is measured by a load cell placed on the retaining wall. On the other hand, surface flow meters are equipped at the front and back of the pile to measure the velocity of the parlite running down. The thickness of the parlite and the condition of motion of the parlite at the time of the impact were photographed using a video camera.

1.2. Test by Artificial Snow

The test equipment consists of a slope, a flow induction wall, a failure box and a retaining wall, similar to that used for the parlite test. (Figure 2)

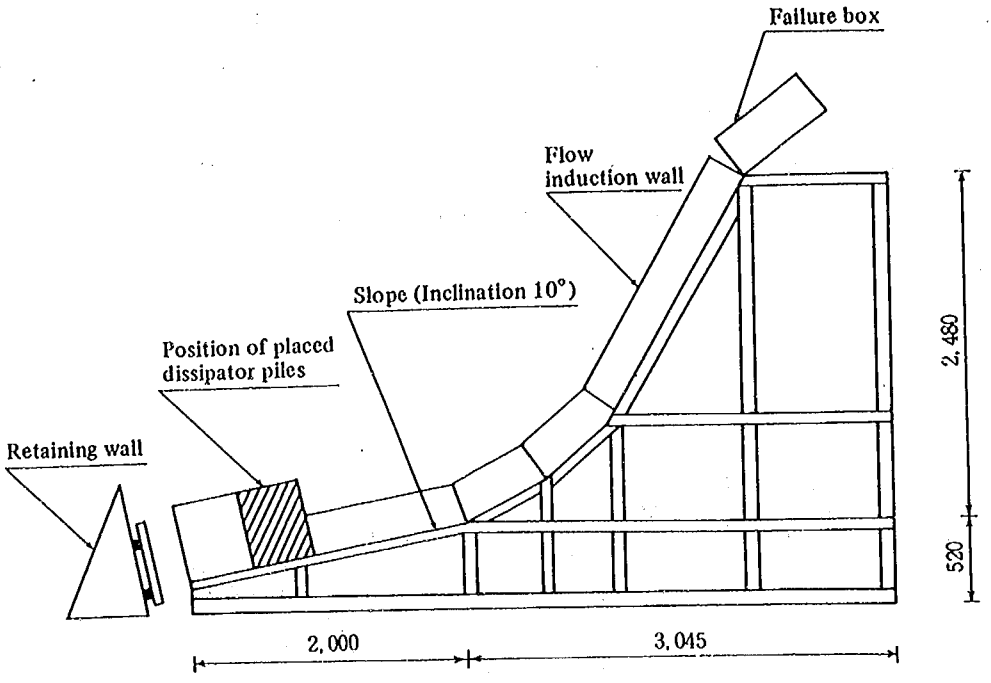

Figure 2. Outline of artificial snow test

In the test, artificial snow of 8 kg (0.02 m^3) produced with an ice slicer is filled in the failure box, which is then placed on the top of the slope. Dissipator piles of a model dissipator are set on the lowest edge of the slope. Measuring instruments such as load cells and flow meters are arranged in a way similar to the parlite test. The test starts when the parting strip in the front of the failure box is removed at the "ready" sign, and the artificial snow is allowed to flow down naturally. The artificial snow collides with the piles placed at the bottom of the slope, at the impact exerted on the dissipator pile is measured with a load cell placed on the pile. After collision, the artificial snow flies away, changes its direction of flow, and is deposited downstream. The impact of the artificial snow colliding with the retaining wall is determined with a load cell equipped on the retaining wall, in a manner similar to the parlite test.

2. Test Cases

The test cases for dissipator piles using parlite and artificial snow are summarized in Table 1. Test cases using artificial snow in which three vertical piles and a model dissipator are shown in Tables 2 and 3 and Photos 1 through 9. The retaining wall in the column of the pile types shown in Table refers to a test in which no dissipator piles are used.

Table 1. Test cases using dissipator piles

Tests using only parlite

Item / Pile type	Pile shape	Pile diameter (mm)	Position of pile (mm)
旗 舰	—	—	—
Vertical pile (1)	Round/ Square	13 28 38	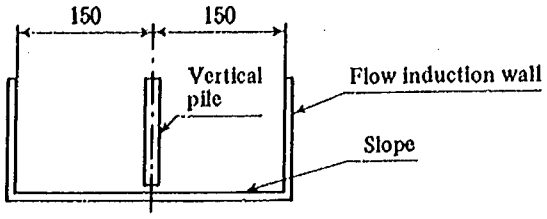
Vertical piles (2)	Round/ Square	13 28 38	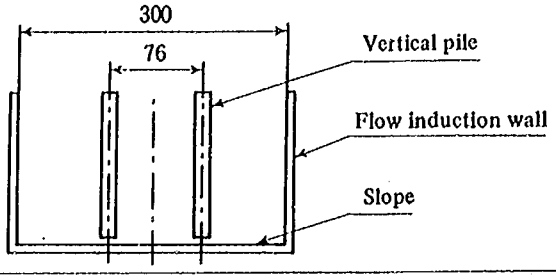
ĸ Lateral pile (1)	Round/ Square	13 19 28	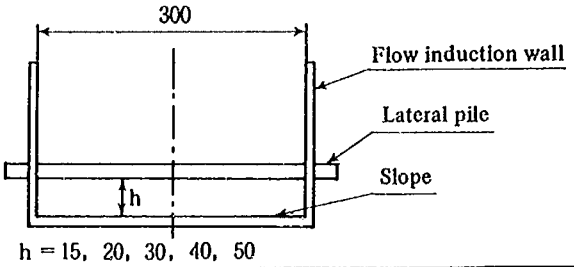 h = 15, 20, 30, 40, 50
Lateral piles (2)	Round/ Square	13 19 28	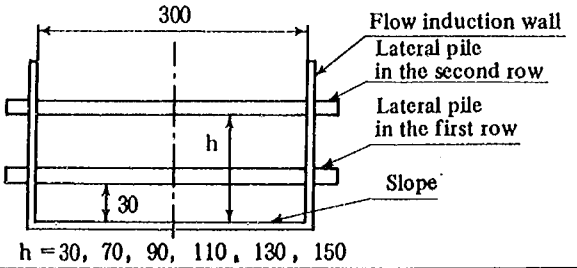 h = 30, 70, 90, 110, 130, 150
Composite pile (1 row)	Round/ Square	13 28	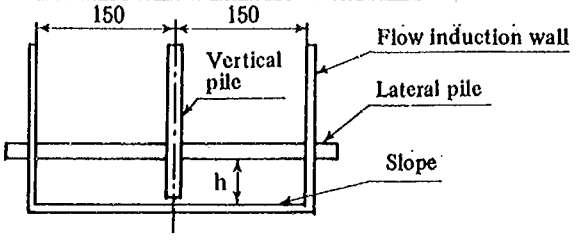 h = 30, 90
Composite pile (2 rows)	Round/ Square	13 28	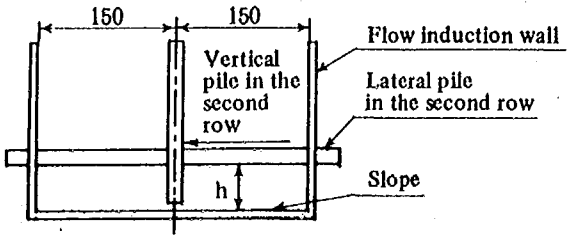 h = 30, 90

Tests using only artificial snow

Items / Pile type	Pile shape	Pile diameter (mm)	Position of pile (mm)
擋　壁	–	–	–
Vertical pile (1)	Round/ Square	13 28	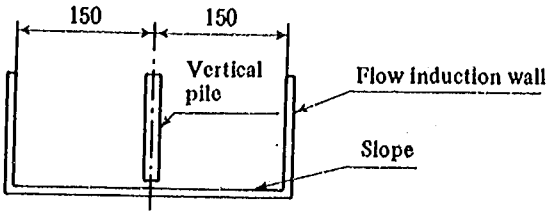
Vertical piles (2)	Round/ Square	13 28	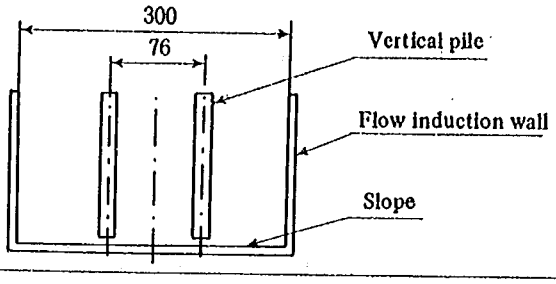
Lateral pile (1)	Round/ Square	13	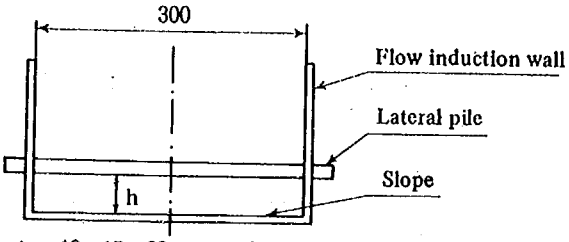 h = 10, 17, 23, 30, 40
Lateral piles (2)	Round/ Square	13	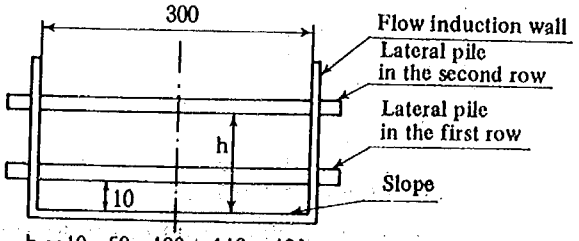 h = 10, 50, 100, 140, 180
Composite pile (1 row)	Round Square	13	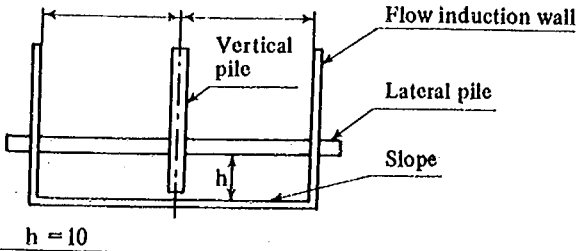 h = 10
Composite pile (2 rows)	Round Square	13	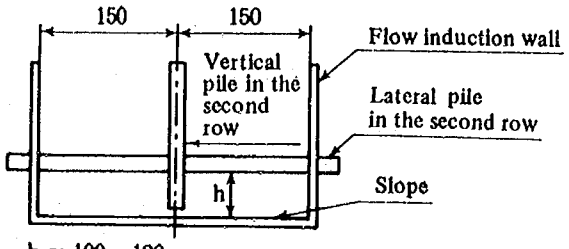 h = 100, 120

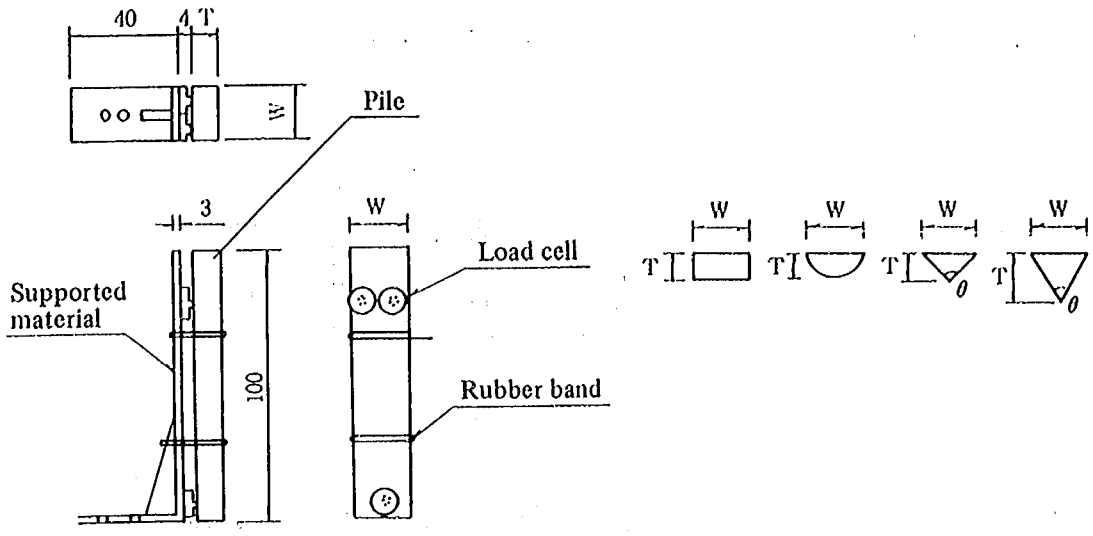

Table 2. Test cases using three vertical piles (arrangement of en equilateral triangle)

Distance of piles		Lateral distance a [cm]					
		4.0	6.0	8.0	10.0	12.0	14.0
Vertical distance b [cm]	0.0				○		
	2.0				○		
	6.0				○		
	8.7	○	○	○	○*	○	○
	12.0				○		
	14.0				○		

Pile height; 10 cm, width; 2 cm,
4 types of shape (square, round and triangle (90° and 60°))

Table 3. Model dissipators (height; 10 cm, width; 50 cm, reinforcing rod diameter; ϕ=14)

Dissipator symbols	Dissipator names	Row number	Porosity [%]	Figure number	Note
A	Shelf type	1	59.2	1–5	One row of EFHI/Photo 1.
B	Shelf type	1	48.7	1–5	
C	Shelf type	1	38.2	1–5	
D	Hurdle type	3		1–6	
E	Jungle gym square type	3		1–7	
F	Jungle gym triangle type	3		1–8	
G	Hurdle type	5		1–9	
H	Jungle gym square type	5		1–10	
I	Jungle gym triangle type	5		1–11	

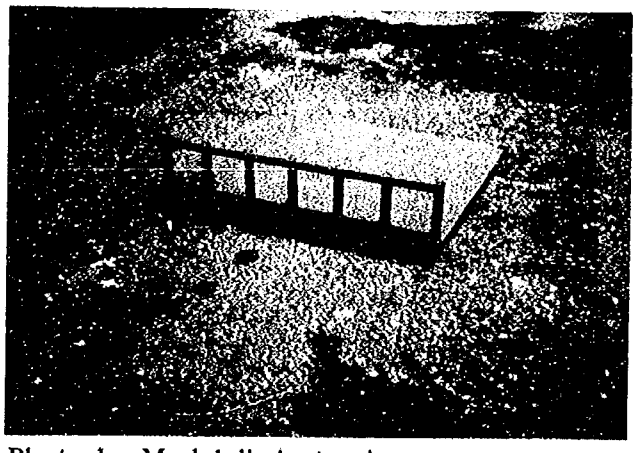

Photo 1. Model dissipator A (one-row shelf type)

Photo 2. Model dissipator B (one-row shelf type)

Photo 3. Model dissipator C (one-row shelf type)

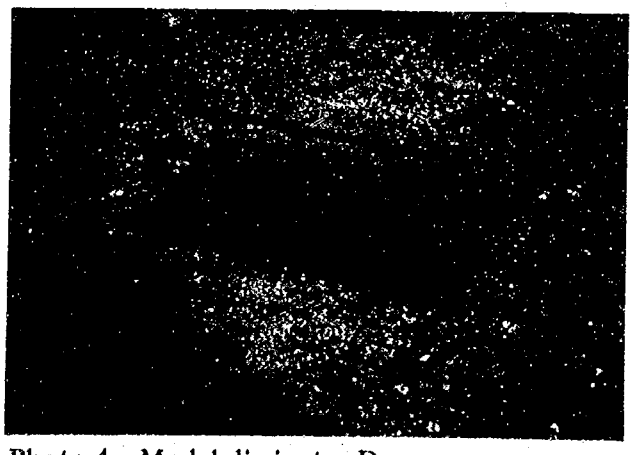

Photo 4. Model dissipator D (three-row hurdle type)

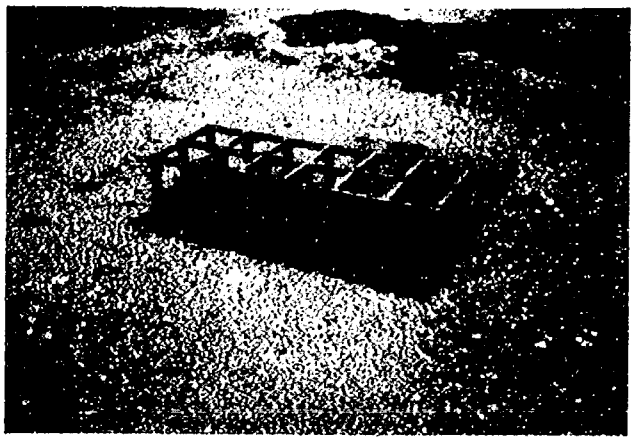

Photo 5. Model dissipator E
(three-row jungle gym square type)

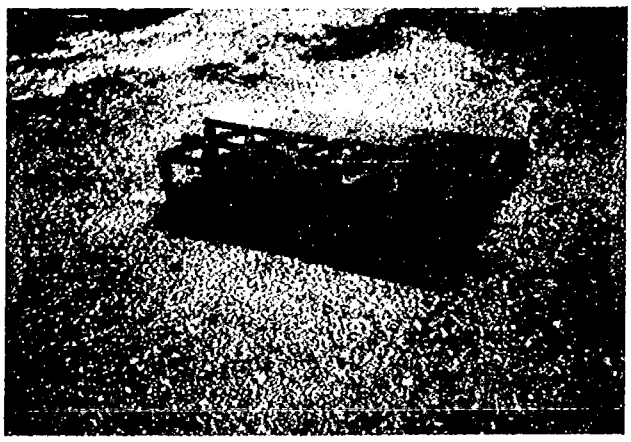

Photo 6. Model dissipator F
(three-row jungle gym triangle type)

Photo 7. Model dissipator G
(5-row hurdle type)

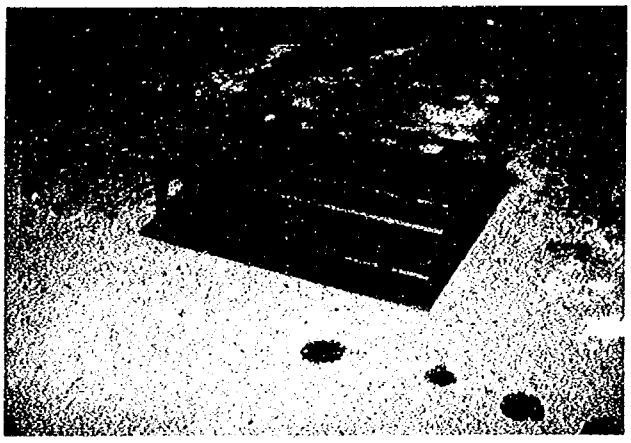

Photo 8. Model dissipator H
(5-row jungle gym square type)

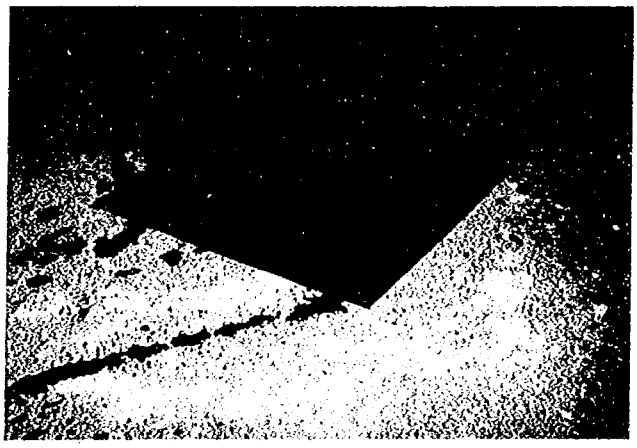

Photo 9. Model dissipator I
(5-row jungle gym type)

3. Test Results

3.1. Parlite and Artificial Snow Tests Using Dissipator Piles

3.1.1. Retaining Wall

The impact exerted by moving parlite or artificial snow on a retaining wall was measured using 4 load cells. Figures 3-(1) and 3-(2) give the total of values measured by the 4 load cells. The bar graphs show the averages of the impact every 0.25 seconds and 0.2 seconds after the occurrence of the impact, and were used to evaluate the impact.

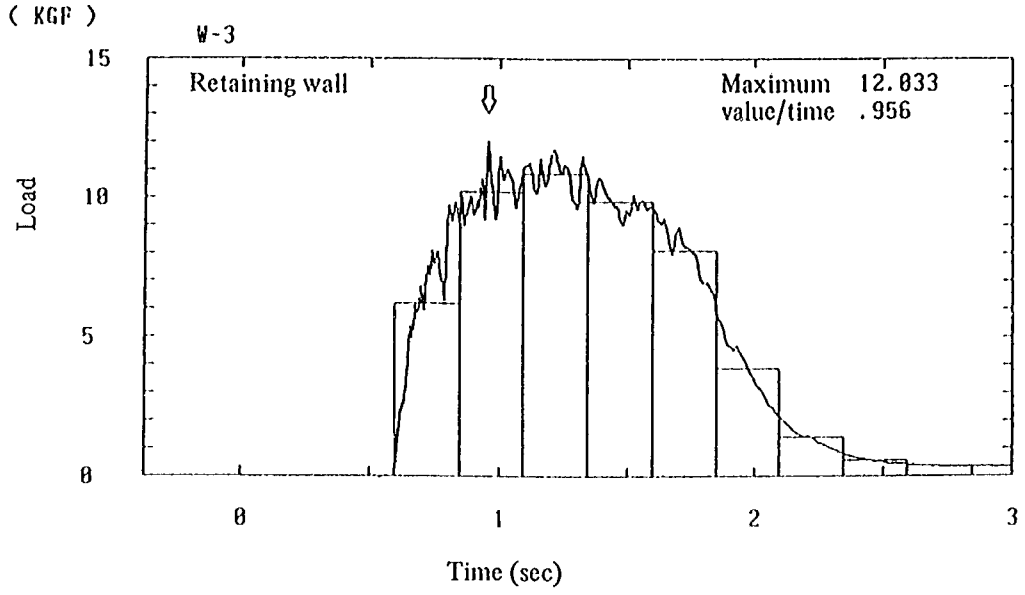

Figure 3-(1) Impact of parlite acting on the retaining wall and the mean values for every 0.25 seconds

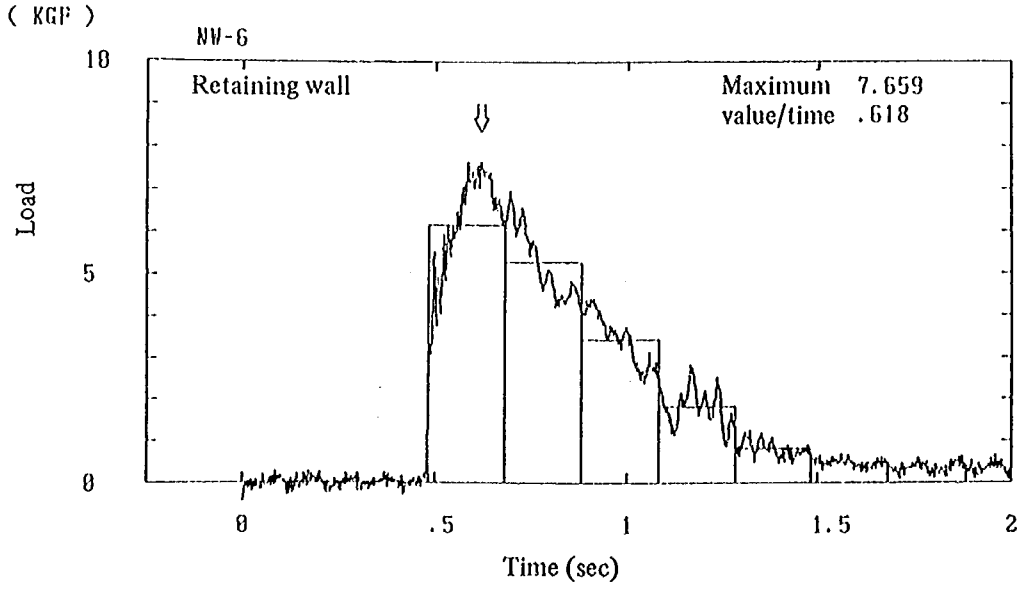

Figure 3-(2) Impact of parlite acting on the retaining wall and the mean values for every 0.2 seconds

A fluid acting on a retaining wall in a flow or moving in a static fluid can generally be evaluated on the basis of the following equation when the flow width is much narrower when compared with that of the retaining wall.

$$P_c = \frac{\gamma}{g} \cdot A \cdot V^2 \quad \cdots\cdots (1)$$

where,

γ : Density of the fluid (t/m^3),

g : Acceleration of gravity, 9.8 (m/sec^2),

A : Action area vertical to the flow direction (m^2),

V : Velocity at the time of collision (m/sec).

The measured values of the impact at collision (means for every 0.25 seconds), and the calculated values on the basis of Equation (1) are shown in Figures 4-(1) and 4-(2), respectively. The figure indicates that the impact acting on the retaining wall is equal to the values calculated on the basis of Equation (1). The impact acting on the retaining wall when an avalanche was simulated parlite or artificial snow can be evaluated by the fluid force shown in Equation (1).

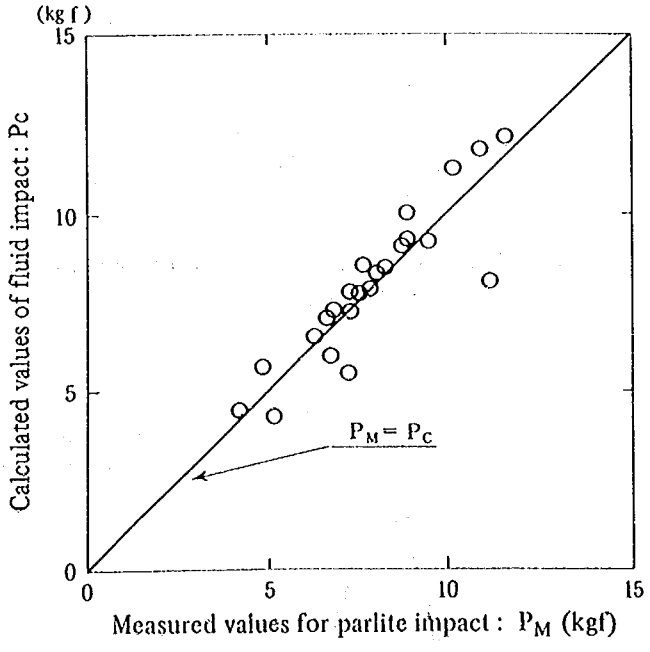

Figure 4-(1) Measured values and calculated values of the impact of parlite acting on the retaining wall

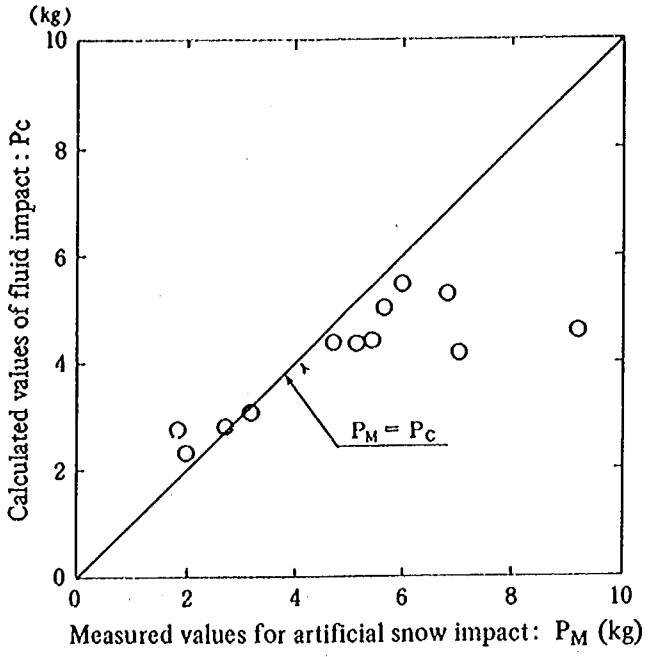

Figure 4-(2) Measured values and calculated values of the impact of artificial snow acting on the retaining wall

3.1.2. Vertical Piles

(1) One Vertical Pile

Generally speaking, a fluid force acting on a relatively simple subject placed in a uniform flow can be evaluated by the following equation.

$$P_c = \frac{\gamma}{2g} \cdot A \cdot V^2 \cdot C \quad \cdots\cdots (2)$$

where C is a coefficient of resistance. This coefficient of resistance varies according to the shape of the receiving surface, the diameter of the receiving surface, the coarseness of the receiving surface, flow velocity, and the physical properties of a fluid material. In this test, a square and round receiving surfaces were used for different diameters of the surface. In addition, the velocity was approximately 4m/s, and the receiving surface was a painted steel pile.

Figure 5 shows the coefficients of resistance obtained from the tests using parlite.

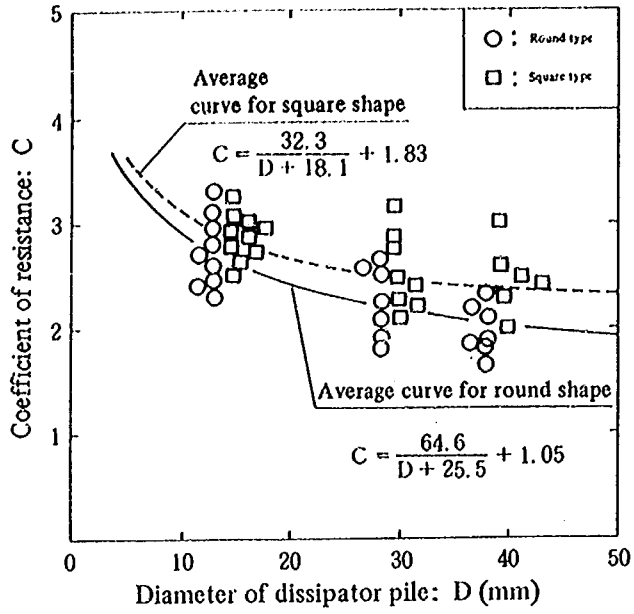

Figure 5. Different coefficients of resistance depending on the pile shape in parlite tests

This figure indicates that the coefficient of resistance for the square type is greater than that for the round type, showing the different characteristics of the impact depending on shape. Furthermore, for both cases, the greater the diameter, the lesser the coefficient of resistance.

The coefficients of resistance for piles in artificial snow cases are shown in Figure 6. In the figure, the coefficients of resistance from the parlite tests are also shown. This figure suggests that the coefficients of resistance from the artificial snow tests are almost equal to those from the parlite tests.

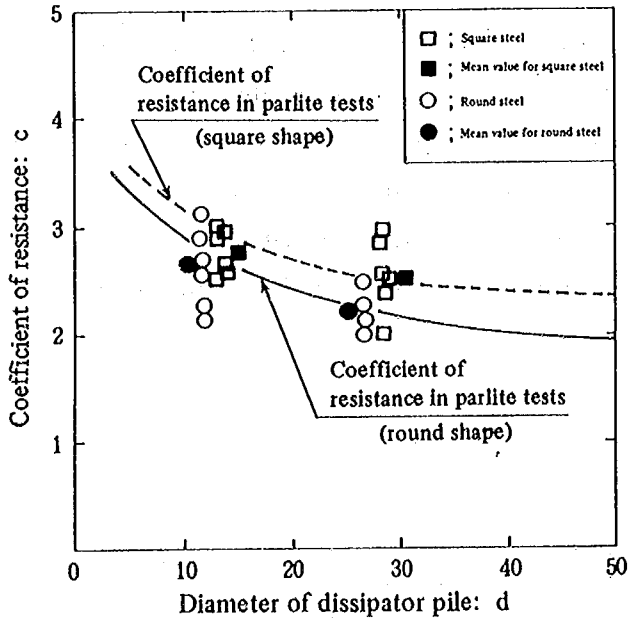

Figure 6. Coefficient of pile shape in artificial snow tests

When moving parlite or artificial snow crashes against the vertical pile, the pile is subjected to an impact which lasts for approximately 1.5 seconds. The impact during this time span is not steady, but varies according to the increase or decrease in the thickness of moving parlite or artificial snow, and the reduction in the velocity. However, the overall effect of an avalanche material on a pile, or conversely the overall effect of the pile on the avalanche material, seems to be evaluated by the physical parameter of the impulse F(t)dt. Figure 6-(1) and 6-(2) show the impulse exerted on the dissipator pile and the retaining wall by the moving parlite and artificial snow, and suggest that the impulse on the pile increases and that on the retaining wall decreases with an increasing diameter for the dissipator pile. The total of these two impulses, however, is constant regardless of the diameter of the dissipator pile.

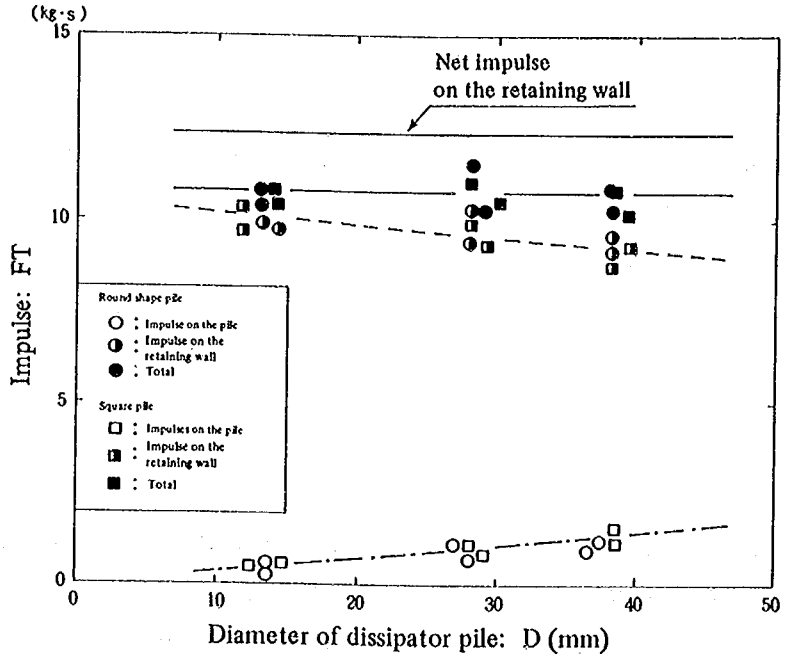

Figure 6-(1) Impulses on the dissipator pile and the retaining wall in the parlite tests. (One vertical pile)

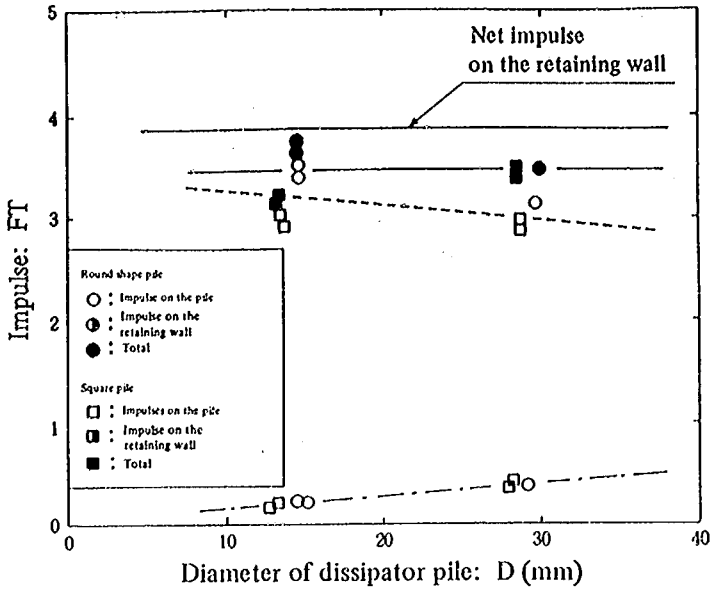

Figure 6-(2) Impulses on the dissipator and the retaining wall in artificial snow tests.

Therefore, the impulse of an avalanche immediately before collision with the dissipator is the sum of the impulse of the avalanche on the dissipator and the impulse of the avalanche after it passes through the dissipator. The equation below for the law of conservation of momentum is therefore valid.

$$\int_0^{t_1} F_1(t)dt = \int_0^{t_2} F_2(t)dt + \int_0^{t_3} F_3(t)dt \quad \cdots\cdots (3)$$

where

F_1 : Avalanche impact immediately prior to collision with the dissipator,

t_1 : Duration of avalanche impact immediately prior to collision with the dissipator,

t_2 : Duration of the avalanche impact acting on the dissipator,

F_3 : Avalanche impact after passing through the dissipator, and

t_3 : Duration of the avalanche impact after passing through the dissipator.

The net impulse on the retaining wall given in Figures 6-(1) and 6-(2) is the impulse on the retaining wall without the placement of piles. Here, the total of the impulses on the pile and the retaining wall is slightly less than the net impulse on the retaining wall. This seems to be due to the loss of impulse at some other places (for instance, the flow induction wall) caused by the placement of vertical piles.

Equation (3) suggests that the greater $F_2(t)dt$ is, the less $F_3(t)dt$ is. That is, a greater avalanche impact on the dissipator pile and a longer duration of the avalanche impact produce a smaller impulse after the avalanche passes through the dissipator. Therefore, the dissipation effect of the vertical pile can be evaluated on the basis of $F_2(t)dt$.

Furthermore, a revision of Equation (3) gives the equation below, which is for the velocity after an avalanche passes through the dissipator.

$$v=\frac{\left(\int_0^{t_1} F_1(t)dt-\int_0^{t_2} F_2(t)dt\right)\cdot g}{m} \quad \cdots\cdots (4)$$

where m is the weight of the avalanche which has paseed through the dissipator. Figures 7-(1) and 7-(2) show the calculated velocities and the velocities measured with a surface flow meter. These figures suggest that both the calculated and measured values are in coincidence, although they have a slight dispersion.

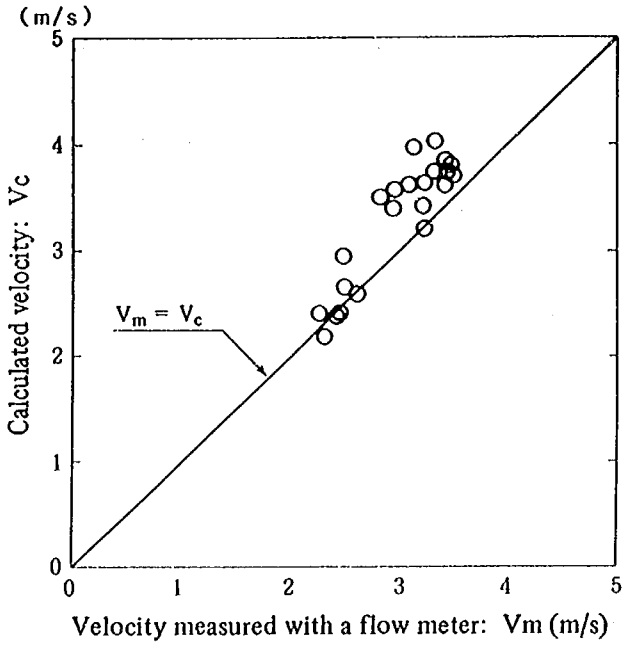

Figure 7-(1) Relation between measured values Vm and calculated values Vc in the parlite tests (on vertical pile)

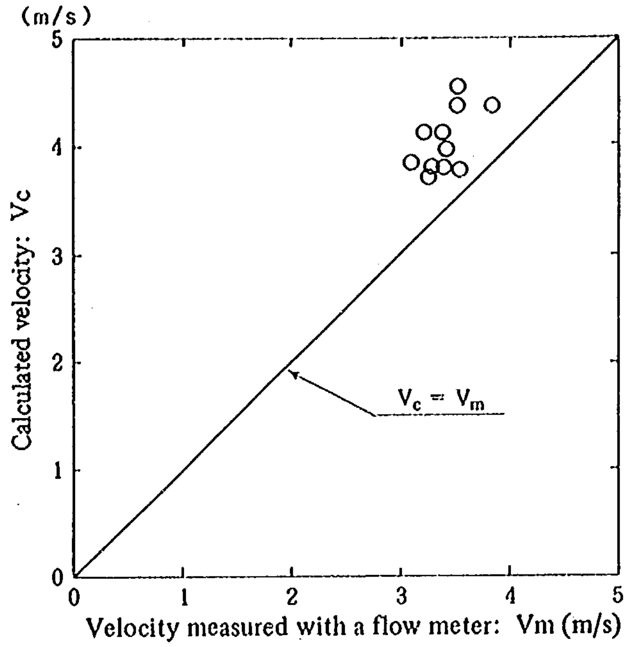

Figure 7-(2) Relation between measured values Vm and calculated values Vc in the artificial snow tests (one vertical pile)

(2) Two Vertical Piles

When two or more piles are joined, the impact exerted on the piles becomes greater than that in the case of a single pile. Generally, this phenomenon is called the blocking effect, and is expressed by the following equation.

$$\varphi=\frac{P_p}{P_s} \quad \cdots\cdots (5)$$

where

φ : Blocking effect,

P_p : Impact on one pile when two or more piles are joined,

P_s : Impact on a single pile.

Figure 8 gives the blocking effect when two vertical piles were used in the parlite tests. The figure indicates that there is no great difference in the rate of blocking effect between the round shape and the square shape. In addition, the blocking effect increases with a smaller W/D, while it decreases with a greater W/D to a constant value. This bending point obtained on the basis of the Casagrande method is W/D=2.5, as shown in the figure.

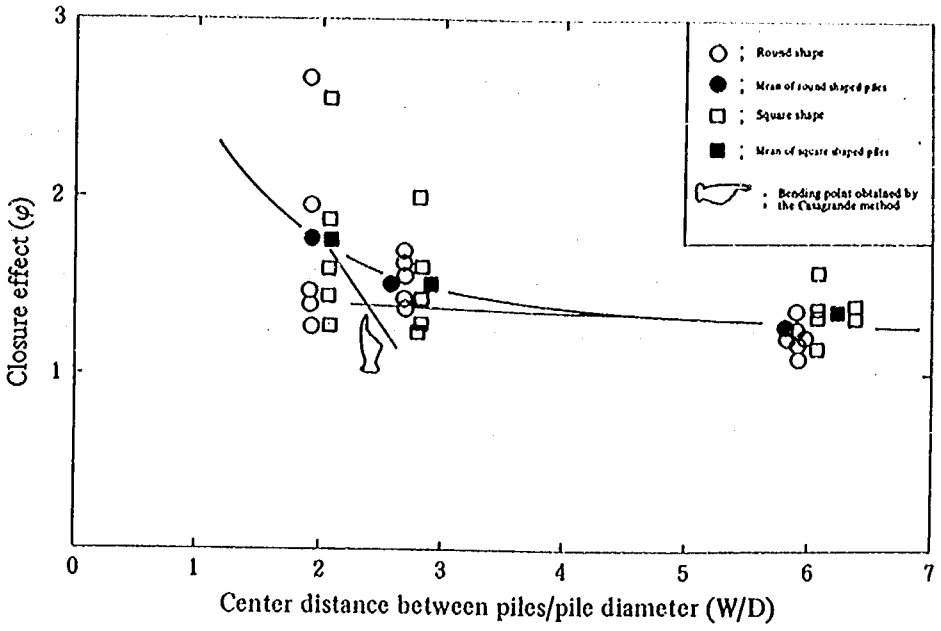

Figure 8. Closure effect in the tests using parlite

Figure 9 shows the blocking effect in the tests using artificial snow. The figure also contains the blocking effect obtained from the parlite tests. The figure indicates that the blocking effect in the parlite tests and the artificial snow tests is in coincidence at W/D=6, while in the artificial snow tests, is less than that in the parlite tests at W/D=2.75. Artificial snow can pass more easily through two adjacent piles than can parlite. This seems to be the reason why the blocking effect in the artificial snow tests is less than that in the parlite tests. No bending point appeared in the artificial snow tests, because no test below W/D=2.5 was done.

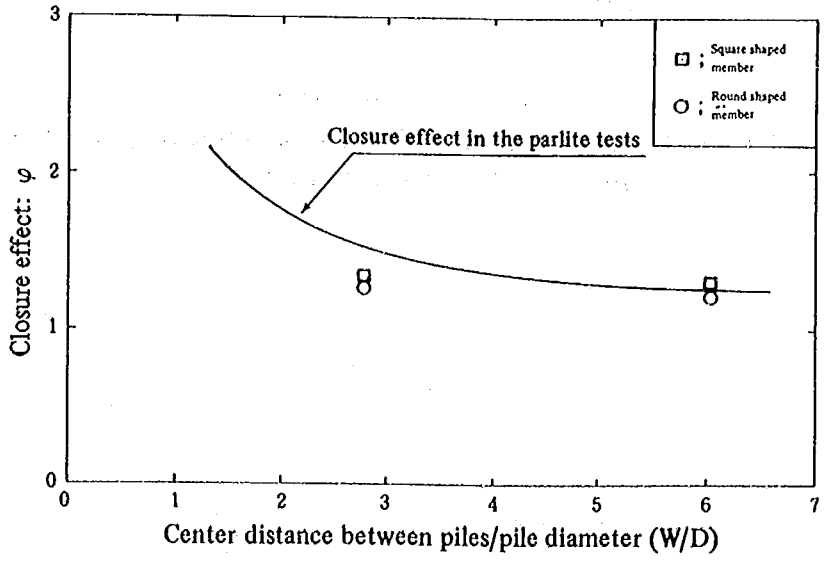

Figure 9. Closure effect in the tests using artificial snow

The impulse in the parlite tests for two piles is shown in Figure 10-(1), which suggests that a greater pile diameter leads to a greater impulse to the piles. On the other hand, the impulse to the retaining wall decreases. This trend is the same with that in the case of one vertical pile. However, the sum of the impulses to the piles and the retaining wall is not constant, but decreases with greater pile diameter. In case of two vertical piles, as mentioned before, the blocking effect appears between the two piles, and parlite deposits between them. The parlite itself therefore forms a kind of wall, which seems to receive the impacts caused by the succeeding parlite. On the other hand, the artificial snow tests as shown in Figure 10-(2), have proved the validity of Equation (3) in the placement of two vertical piles.

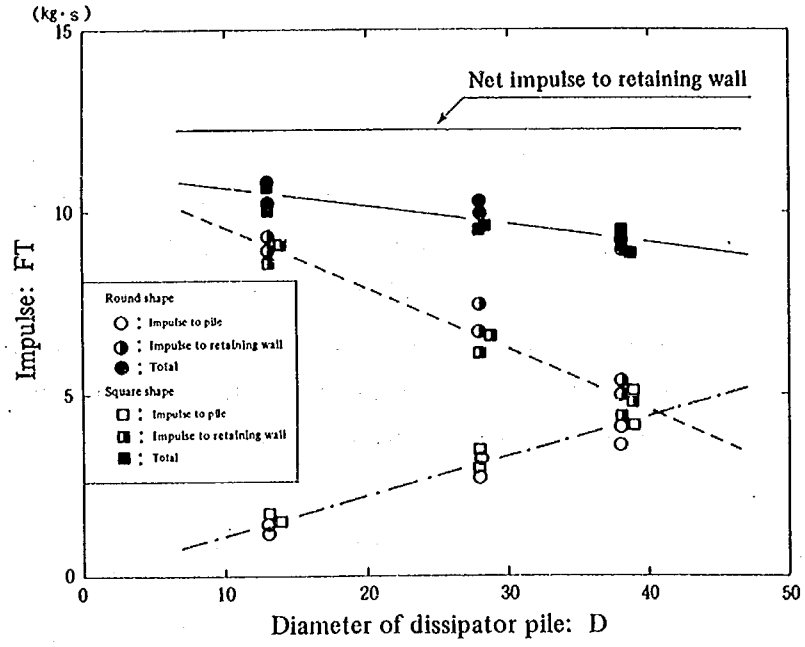

Figure 10-(1) Impulses to energy dissipator and retaining wall in the parlite tests (Two vertical piles)

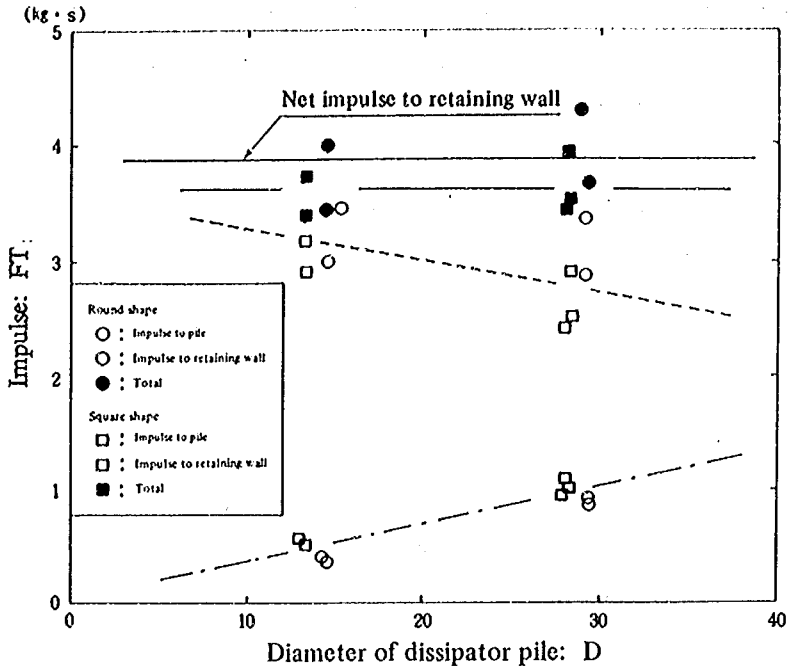

Figure 10-(2) Impulse to retaining wall in the artificial snow tests (Two vertical piles)

3.1.3. Lateral Pile

(1) One Lateral Pile

In the parlite tests, the moving parlite becomes thicker by the placement of a lateral pile, as shown in Figure 11, resulting in the lower density at the time of collision with the lateral pile. Then, the parlite impact acting on the lateral pile is expressed by the equation below:

$$P_c=\frac{\gamma}{2g}\cdot A\cdot V^2\cdot C\ L \quad \cdots\cdots (6)$$

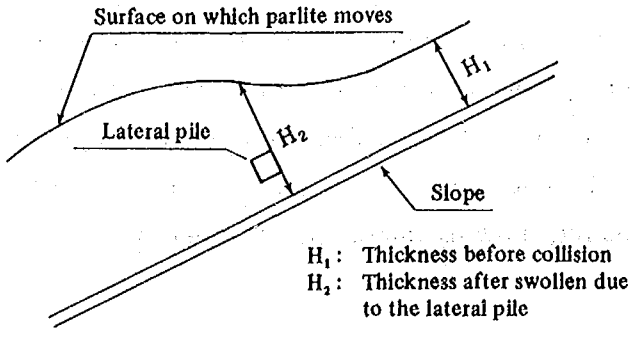

Figure 11. Density changes due to lateral pile placement

The L values obtained in this test are shown in Figure 12. The ratio of thickness (H_1/H_2) shown in Figure 11 are also given in this figure. The figure suggests that there is nearly no difference in the L values between the two different shapes, and that the L value decreases with the larger pile diameter. Furthermore, the ratio of thickness (H_1/H_2) is equal to the L value. This indicates that the impact on the lateral pile decreases with a changing thickness of the parlite, due to placement of the lateral pile (decreases density).

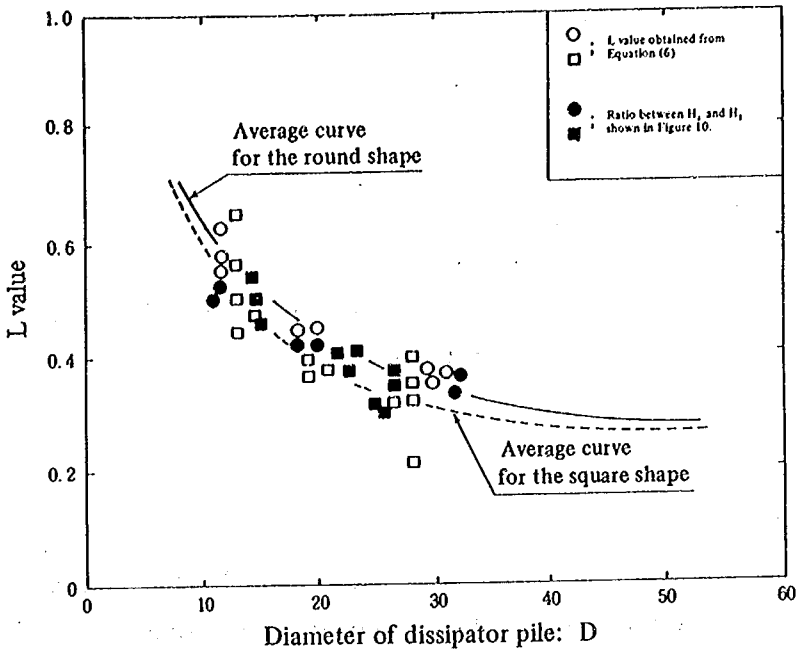

Figure 12. L value (one lateral pile)

In contrast, unlike the parlite tests, the artificial snow tests did not show thickness changes and the impact on the dissipator pile was expressed by Equation (2).

Figures 13-(1) and 13-(2) show the impulses of the avalanche impact acting on one lateral pile and the retaining wall. Figure 13-(1) suggests that the impulses for the round shape and the square shape are equal in the parlite tests. In Figures 13-(1) and 13-(2), the impulse on the pile is nearly proportional to the pile diameter, and the impulse on the retaining wall is inversely proportional to the pile diameter. In addition, the sum of these two values is constant regardless of the pile diameter, showing the validity of Equation (3).

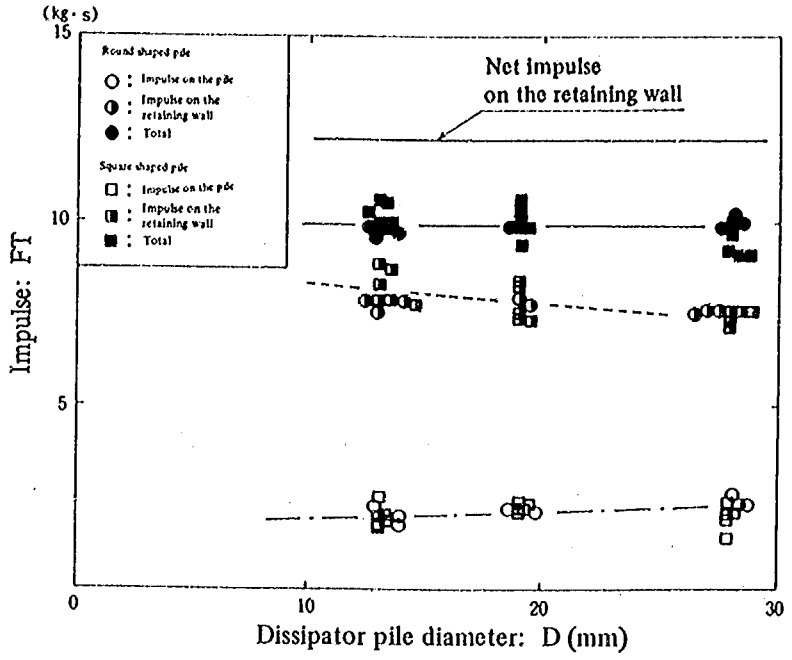

Figure 13-(1) Impulse on the dissipator pile and the retaining wall in the parlite tests
(Impulse on one lateral pile)

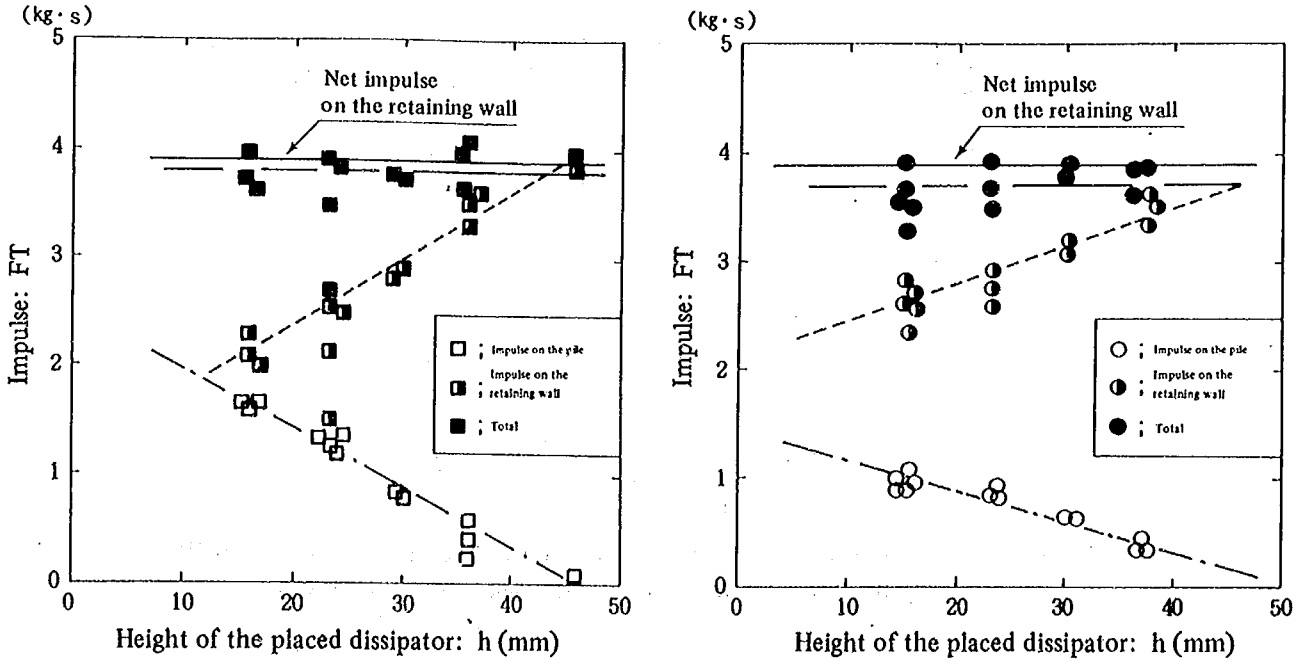

a) Square shape b) Round shape

Figure 13-(2) Impulse on the dissipator pile and the retaining wall in the artificial snow tests (one lateral pile)

(2) Two Lateral Piles

An additional lateral pile was placed behind one lateral pile (placement height of 3 cm) to examine the impact acting on the back lateral pile and the dissipation effect. Figures 14 show the impulses for the impact on the lateral piles in the first and second rows. As shown in these figures, the back row pile is placed at the same height as the front row pile, and then the back lateral pile is subjected to nearly no impact, but a higher height of placement results in a greater impact. When the back lateral pile is placed even higher, the impact on the back lateral pile decreases. The maximum impact received by the back row pile is located at h=8.0 in the parlite tests, and at h=9.0 cm in the artificial snow tests. The major direction of flying away due to the first row lateral pile (flying angle) is approximately 40°. The impulse on the second row lateral pile is much smaller than that on the first row pile, and the lateral pile in the second row is thus not so effective in dissipating the avalanche energy.

Figures 15-(1) and 15-(2) show the total impulse on the dissipator consisting of two lateral piles and the retaining wall, proving the validity of Equation (3).

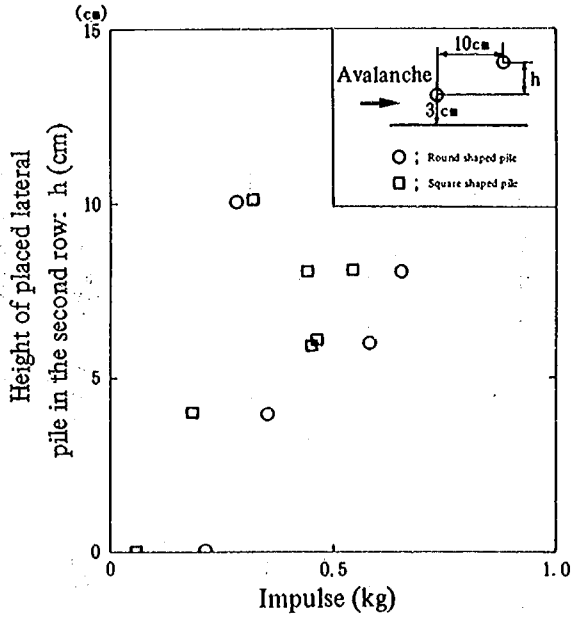

Figure 14. Distribution of impulse towards the vertical direction in the parlite tests (Lateral pile in the back row: 13 mm)

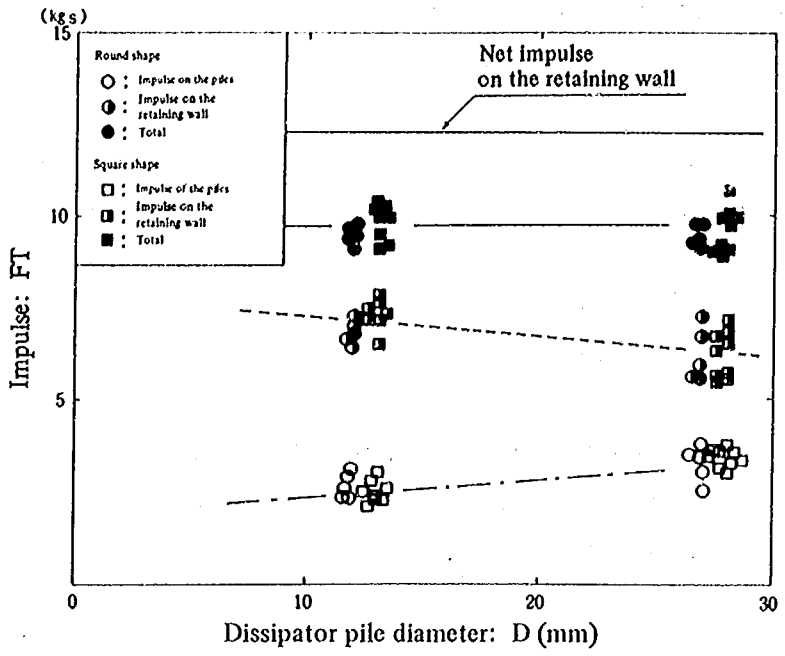

Figure 15-(1) Impulse on the dissipator and the retaining wall in the parlite tests (two lateral piles)

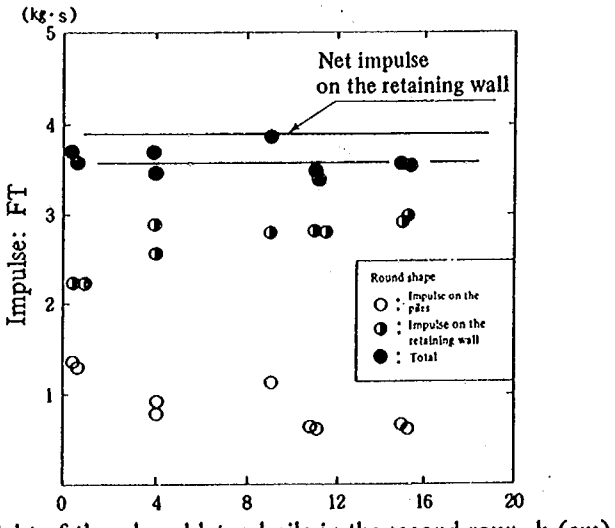

a) Round shape

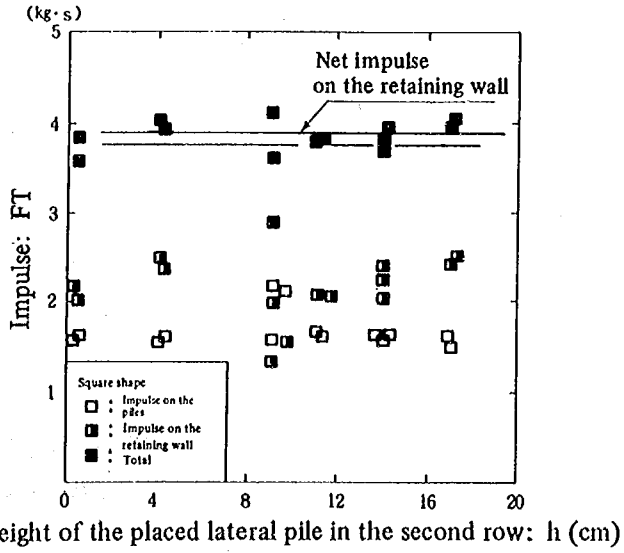

b) Square shape

Figure 15-(2) Impulse on the dissipator and the retaining wall in the artificial snow tests (two lateral piles)

3.1.4. Composite Piles (One Row and Two Rows)

The composite pile tests, where both a vertical pile and a lateral pile are placed, is a simulation of an actual dissipator. Figures 16-(1) and 16-(2) show the impulse on the composite piles and that on the retaining wall. These figures indicate that the impulse received by the dissipator dicreases with a greater diameter of the dissipator pile, and that the impulse on the retaining wall decreases. Nevertheless, the total impulse on these two is constant. This proves that Equation (3) is valid for a model with a more complicated arrangement of piles. In addition, Figure 16-(2) shows that the impulse on the piles does not differ between the one-row arrangement and the two-row arrangement in the aritificial snow tests. Figure 16-(3) shows that the impulse on the piles in the second row is much smaller than that in the parlite tests, showing that the second row piles have no effect in dissipating the avalanche energy.

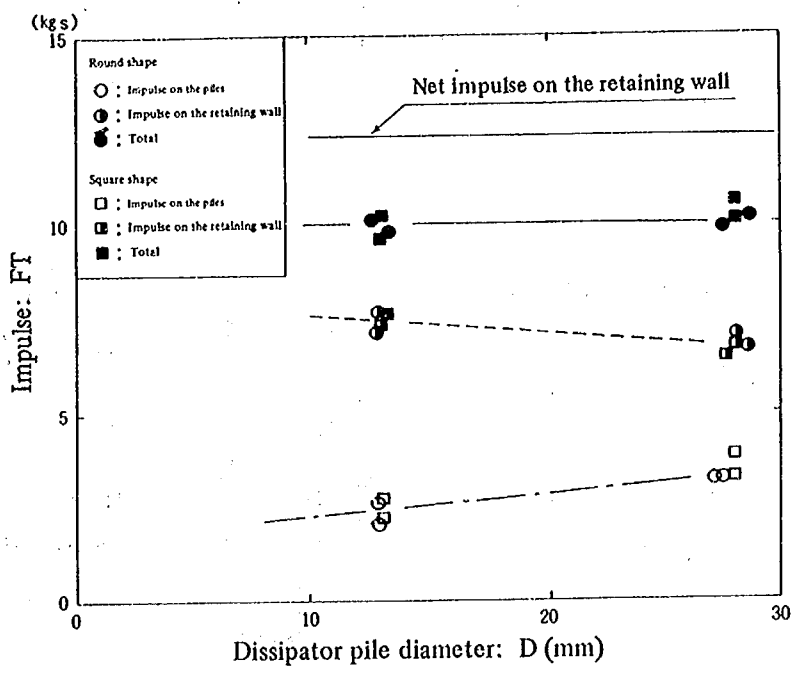

a) One-row composite piles

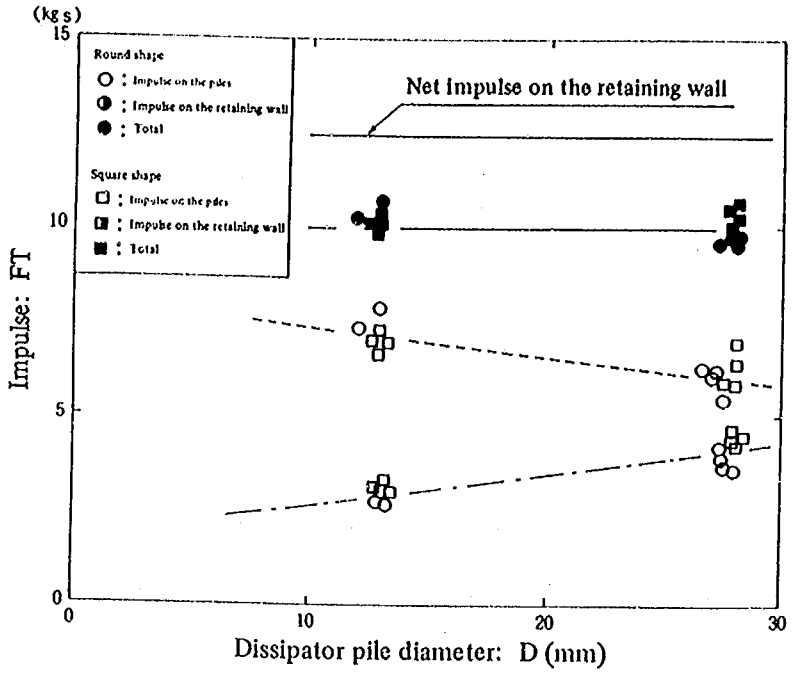

b) Two-row composite piles

Figure 16-(1) Impulse on the dissipator and the retaining wall in the parlite tests

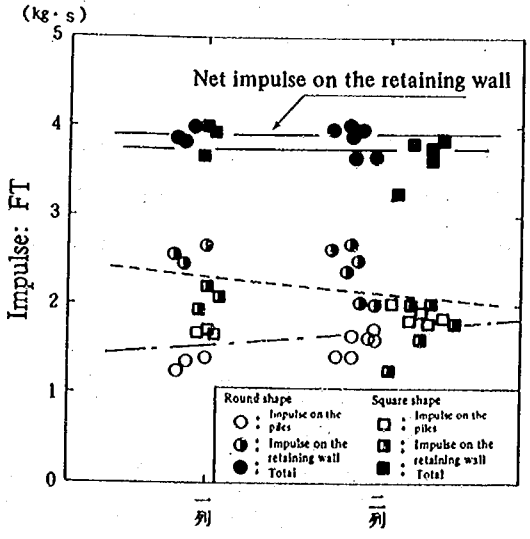

Figure 16-(2) Impulses on the dissipator and the retaining wall in the artificial snow tests

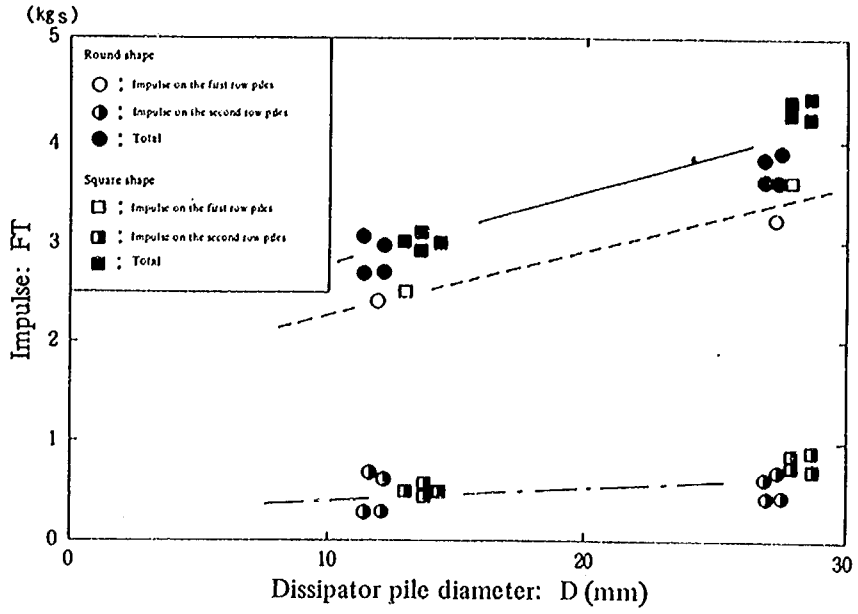

Figure 16-(3) Impulses on the first row piles and the second row piles in the parlite tests

3.2. Artificial Snow Tests Using Three Vertical Piles (Equilateral Triangle Arrangement)

In order to understand the impact characteristics on composite piles, a comparison was made between the mean impact acting on two vertical piles on the upstream (hereinafter refered to as left and right piles) and the impact acting on one vertical pile on the down-stream (hereinafter refered to as the central pile). See Section 2. Test Cases (Table 2) for the conditions of arrangement.

To start with, the impact characteristics associated with a changing lateral distance between the left and right piles, when the vertical distance between the left and right piles and the central pile is kept constant (b=8.7 cm), are shown in Figures 17-(1) through (4). The test results on the

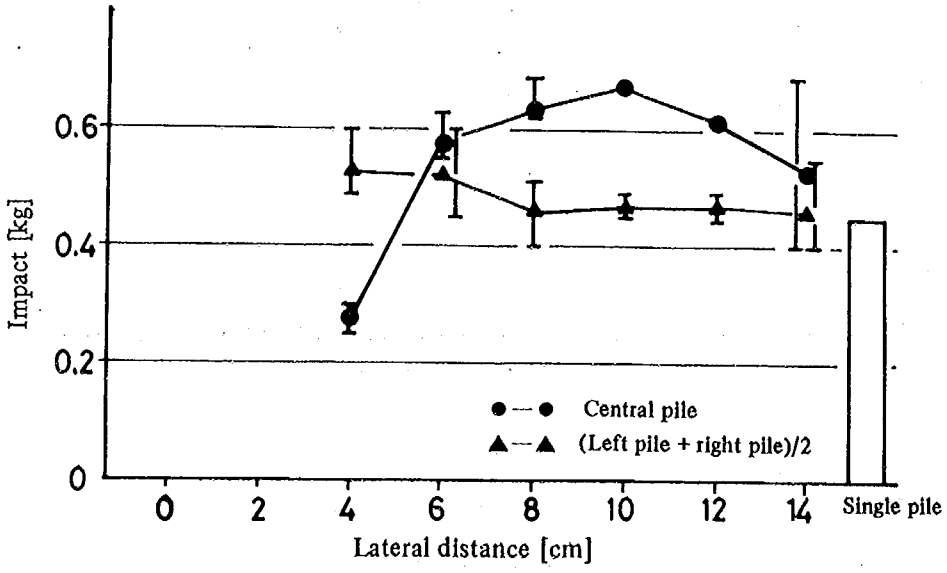

Figure 17-(1) Impact on more than one pile, by lateral distance (square)

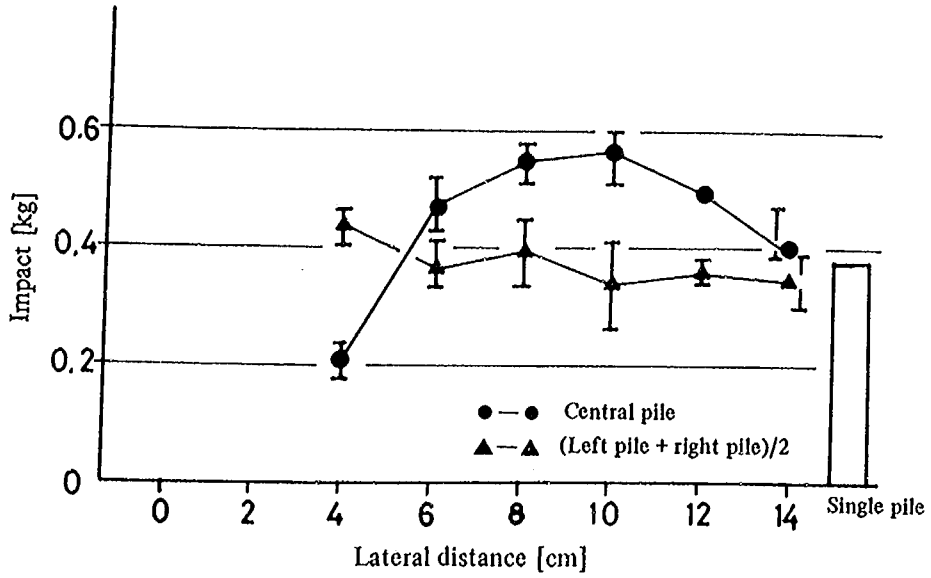

Figure 17-(2) Impact on more than one pile, by lateral distance (round)

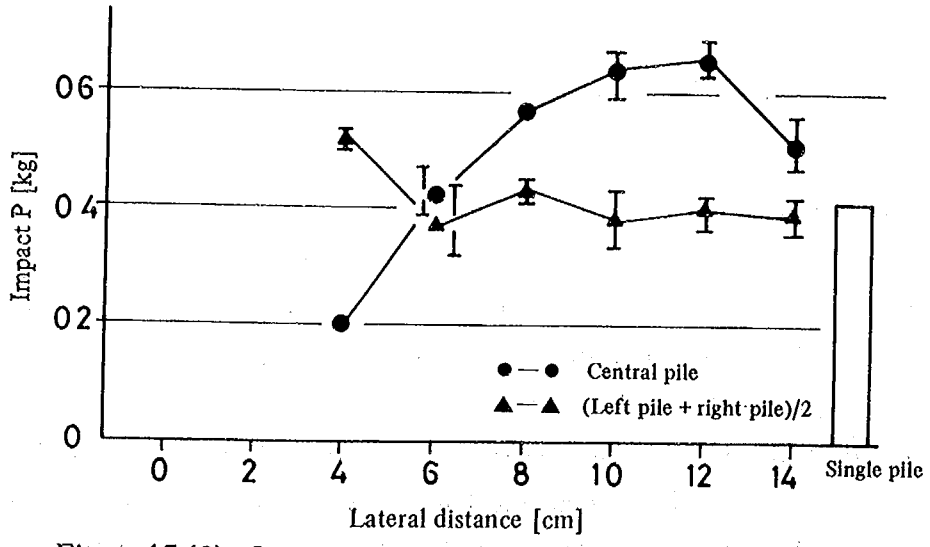

Figure 17-(3) Impact on more than one pile, by lateral distance (triangle: vertical angle 90)

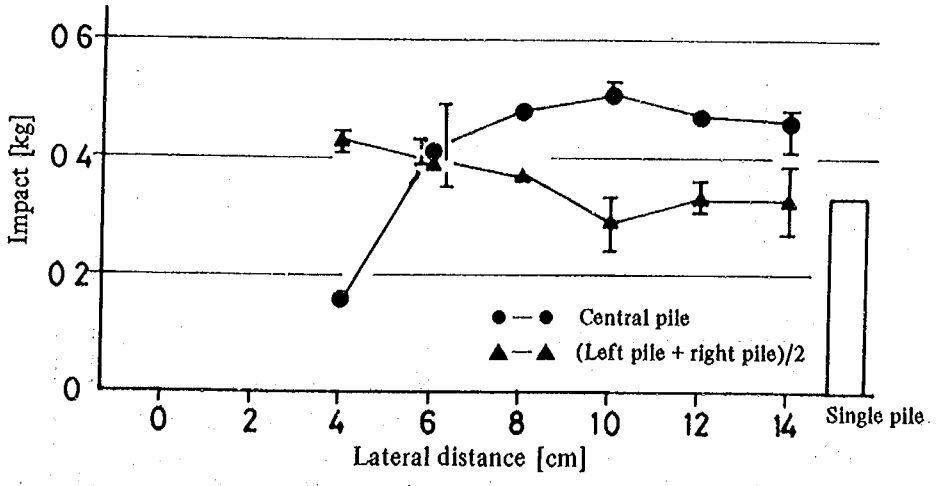

Figure 17-(4) Impact on more than one pile, by lateral distance (triangle: vertical angle 60)

impact acting on one pile in each shape are added on the right corner for reference. The mean values for both the left and right piles were similar to those from the test on a single pile for each shape, while they tended to increase with a narrower lateral distance. This seems to be due to the manifestation of the blocking effect between the piles, when the pile distance becomes narrower. With respect to the central pile, a convex form with the maximum near the 10 cm lateral distance was recognized for each shape. An experimental equation obtained on the assumption that this convex form is an equation of the secondary degree, produced the results shown below:

Front shape of vertical pile		Secondary regression equation	Correlation coefficient	P maximum lateral distance [cm]
Square	:	$P=(-1.11a^2+21.94a-39.51)/100$	$R=0.896$	$a_m=9.9$
Round	:	$P=(-1.07a^2+20.70a-42.56)/100$	$R=0.942$	$a_m=9.7$
Triangle (vertical angle 90)	:	$P=(-1.04a^2+22.11a-52.59)/100$	$R=0.980$	$a_m=10.6$
Triangle (vertical angle 60)	:	$P=(-0.78a^2+16.53a-34.99)/100$	$R=0.955$	$a_m=10.6$

P: Impact

a: Lateral distance between the left pile and right pile [cm] $(4 \leqq a \leqq 14)$

This result shows that under these test conditions the greatest impact acts on the central pile, when the lateral distance is 10 cm (regular triangle arrangement). In addition, there is a tendency for there to be an extremely small impact value when the lateral distance becomes 4 cm. This seems to be because the above-mentioned blocking effect results in a narrower avalanche flow passing through between the left and right piles.

Figures 18-(1) through (4) show impacts when the vertical distance between the left and right piles and the central pile, while keeping the lateral distance between the left and right piles constant (a=10 cm). In these figures, the case of b=0 cm means that the left and right piles and

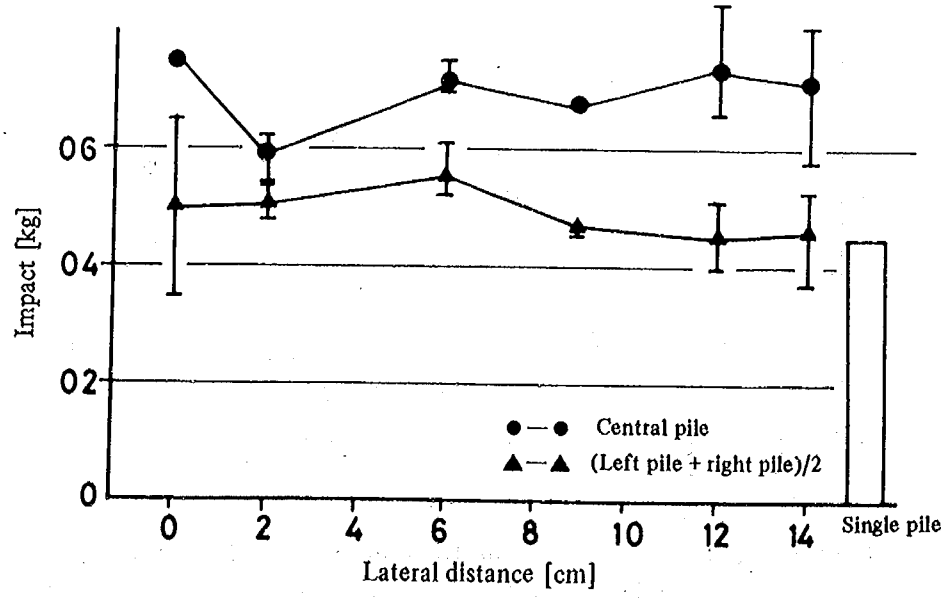

Figure 18-(1) Impact on more than one pile, by vertical distance (Square)

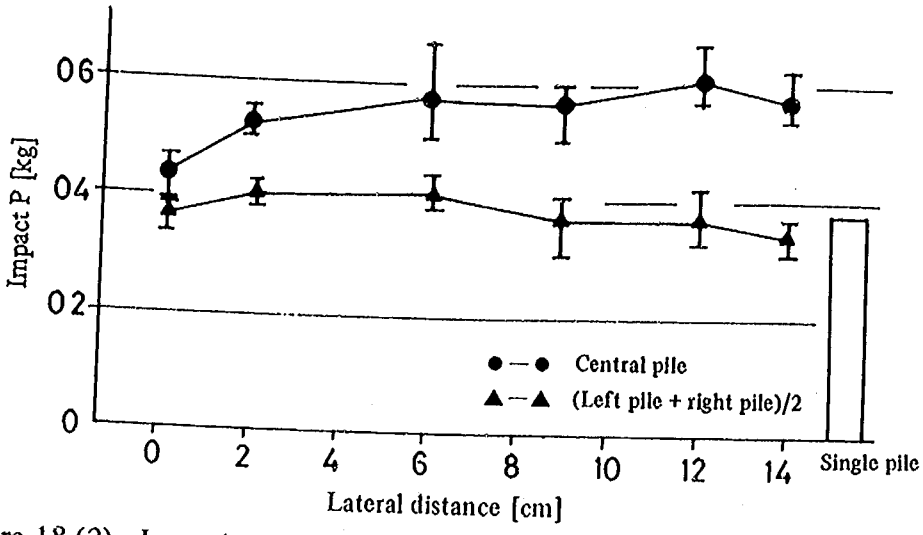

Figure 18-(2) Impact on more than one pile, by vertical distance (Round)

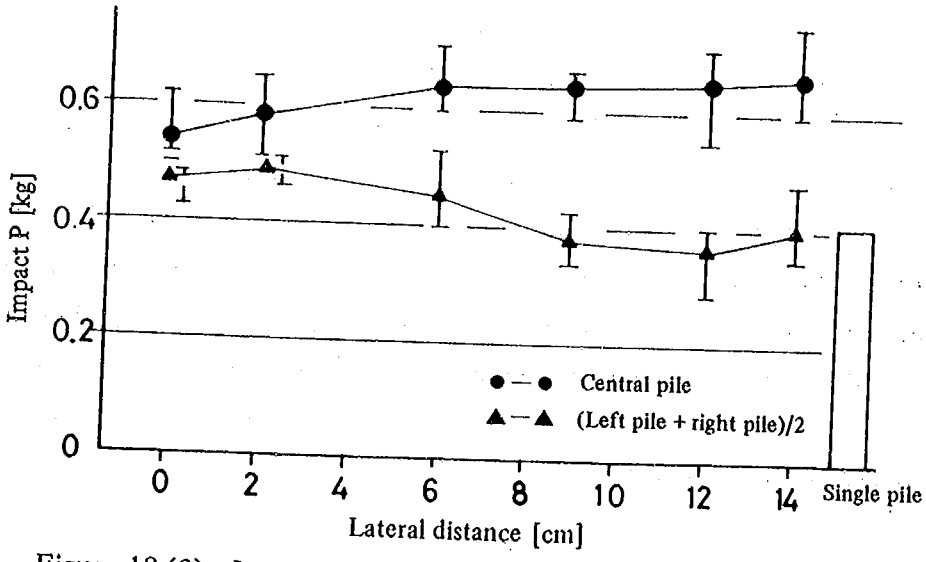

Figure 18-(3) Impact on more than one pile, by vertical distance (triangle: vertical angle 90)

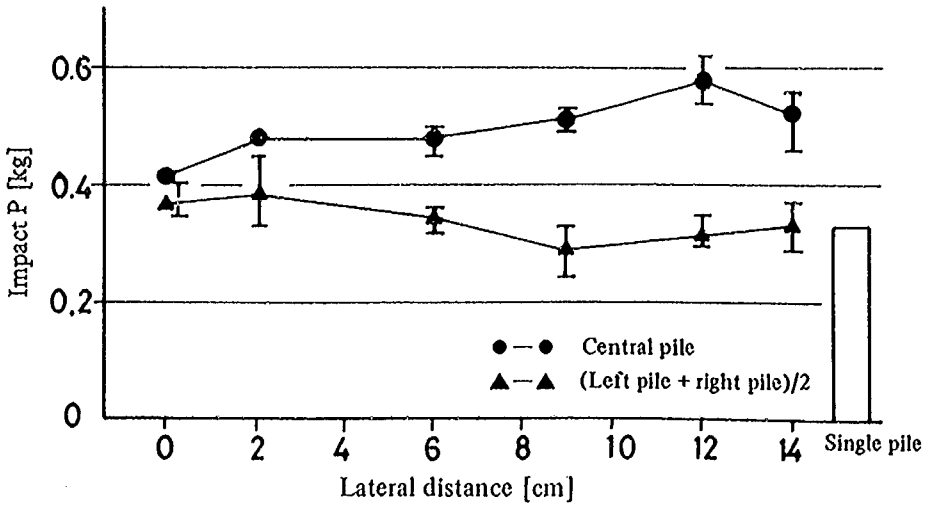

Figure 18-(4) Impact on more than one pile, by vertical distance (triangle: vertical angle 60)

the central pile are placed in a linear line. Observing the impacts by vertical distance from the left and right piles, it is clear that for each shape, the impact is almost the same with that on a single pile, when the distance is wider than 8.7 cm, with there being no effect of the central pile. However, a tendency for the impact to increase below an interval of 6 cm is recognized. This seems to be because the shorter vertical distance results in an intrusion of the central pile into the left and right piles, among which the blocking effect manifests. The central pile receives a greater impact than the left and right piles as a whole. In addition, the impact on the central pile tends to decrease with a narrower vertical distance in contrary to the cases of the left and right piles. This seems to be because the central pile receives an impact like the left and right piles when the vertical distance is short, but it receives the entire avalanche flow narrowed by the left and right piles when the vertical distance is wider. Therefore, when the central pile is moved from the position of the one lateral row arrangement with the left and right piles towards the downstream under this test conditions, the impact on the central pile decreases and then becomes constant above a certain limit.

3.3. Tests Using Model Dissipators

The impact acting on the retaining wall placed at the lower end, when a model dissipator was set (see 2. Test Cases (Table 3 and Photos 1 through 9 for shapes), tended to become extremely small in comparison with a case of no measure (8.37 kg on the average) (Figure 19).

Figure 20 illustrates the porosity (transmissivity of an avalanche flow) of the dissipators A, B and C (considered as a protection fence) and the impact acting on these dissipators. This figure indicates that increasing porosity results in an exponential increase in the impact acting on the retaining wall placed at the downstream end. In these models used in this study, the number of lateral piles was changed while keeping the number of vertical piles constant to

change the porosity. Therefore, placement of more lateral piles seems to intensify the dissipation effect.

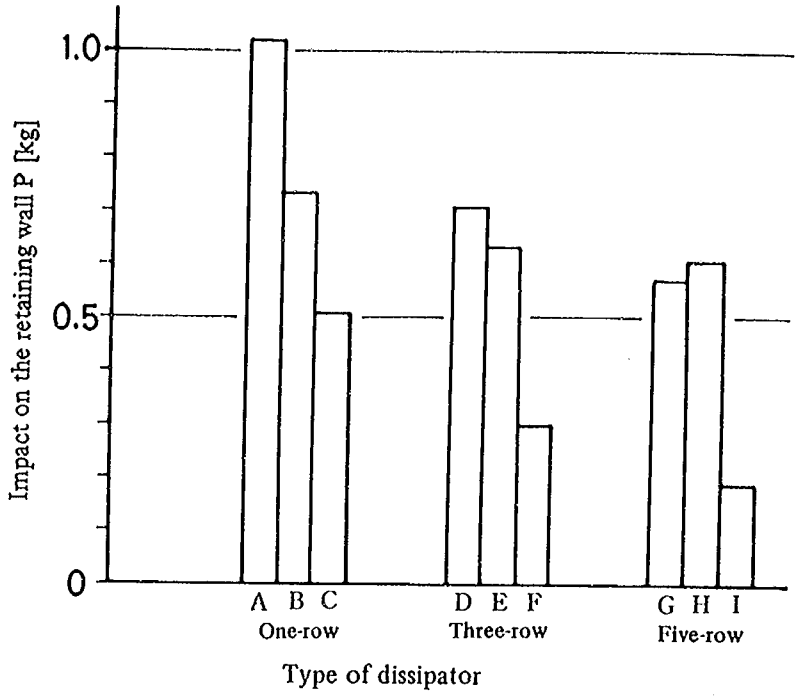

Figure 19. Impact on dissipator by type

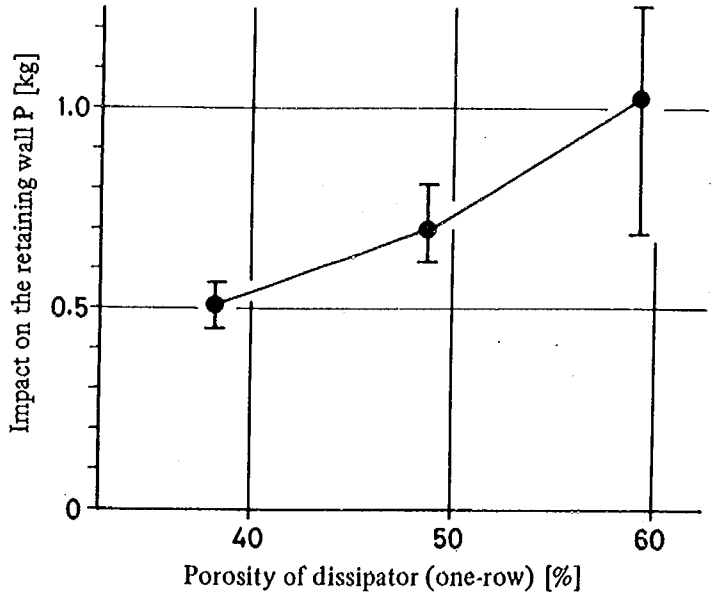

Figure 20. Porosity of the one-row dissipator (shelf) and impact on the retaining wall

In the cases of the three row dissipator and the five row dissipator (Figure 21), the hurdle type and the square type gave a similar value, while the jungle gym type showed an extremely small value. Then, the snow deposit after an avalanche flow had passed through was measured, and the results summarized in Table 4. This table indicates that the jungle gym type recorded the greatest deposit particularly in the fifth row, where more than half of the quantity of flowing snow was deposited. Therefore, a little amount of snow crushed against the retaining wall, assumedly resulting in a smaller impact value.

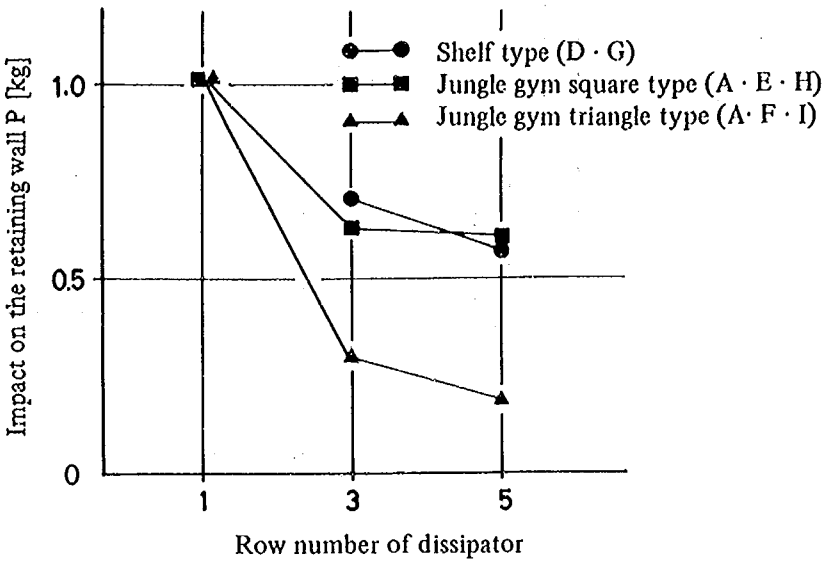

Figure 21. Effects of dissipator by the row number

Table 4. Deposits within dissipators

Sign of dissipator		Snow deposit within dissipator [cm]	Deposit percentage [%]
Three rows	D	little	0.0
	E	2,417	12.6
	F	3,389	17.7
Five rows	G	2,016	10.5
	H	4,207	21.9
	I	11,467	59.7

Figure 21 shows that the impact on the retaining wall with respect to the effects of the number of row in dissipators. This figure indicates a tendency for an increasing number of rows to lead to a lesser impact, but there was no extreme difference between the third and the fifth rows. This seems to be due to lessened effectiveness of the fourth and fifth rows, because the flying condition clearly indicated that the avalanche flow was dispersed during the first three rows.

The maximum snow dispersion heights due to the dissipators are given in Figure 22. According to this figure, the maximum height is approximately 50 cm for each dissipator, with no clear difference among them. Next, the maximum distance that snow flew due to the dissipators (Figure 23) shows a tendency similar to the impact on the retaining wall (Figure 19). Then, the maximum snow flying distances and the impacts are compared as shown in Figure 24, which indicates that the snow flying distance tends to be proportional to the impact, because the snow flying height was also the same in these tests. In this figure, a point downwards to the left side indicates the higher dissipation effect, and the jungle gym triangle type thus showed the highest dissipation effect.

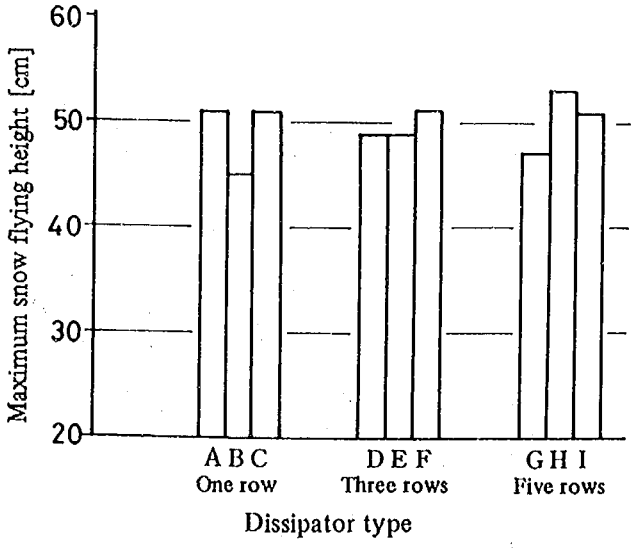

Figure 22. Snow flying height due to dissipator

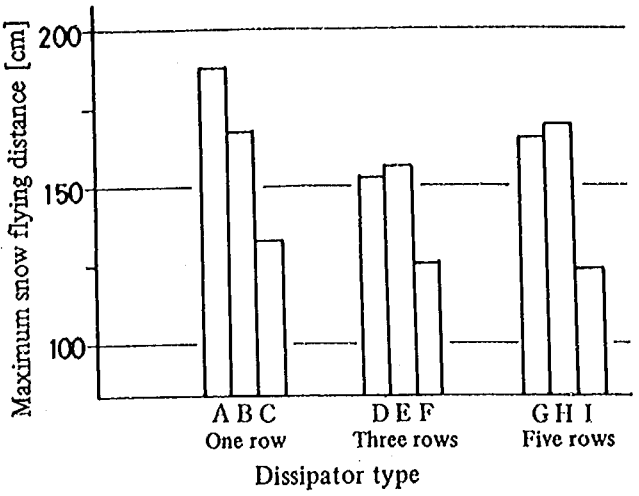

Figure 23. Snow flying distance due to dissipator

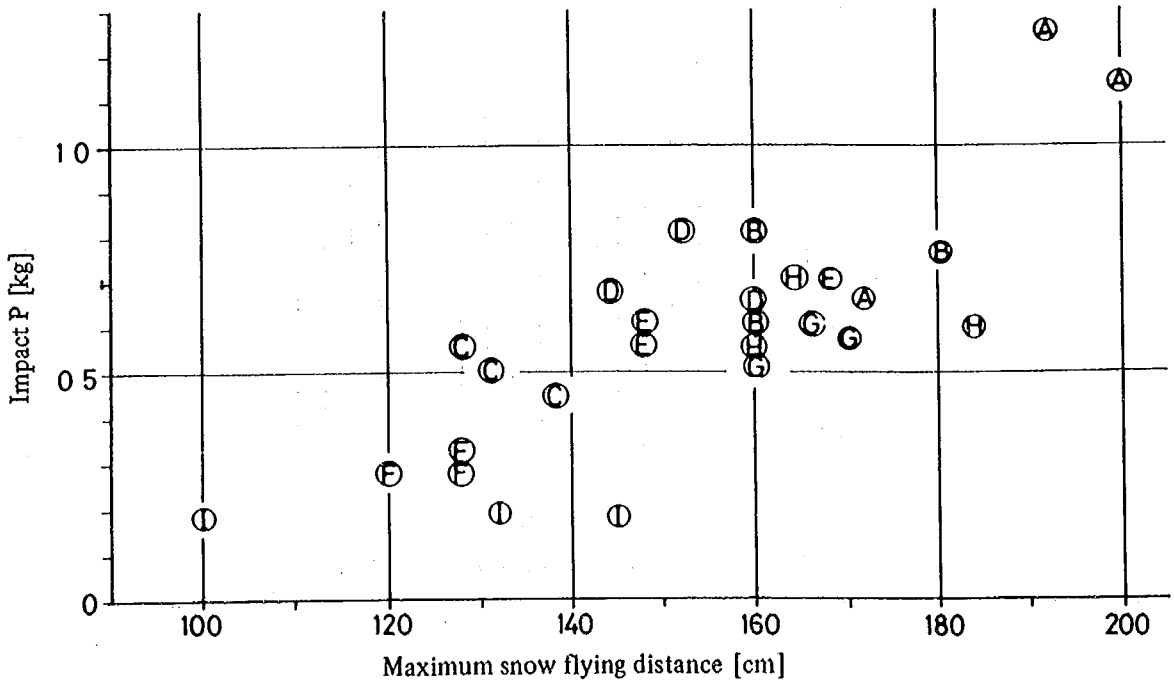

Figure 24. Snow flying distance due to dissipator and the impact

4. Future Prospect

This study made it clear that within a small scale range where no closure effect appears, the impact acting on a dissipator pile can be evaluated using a fluid equation. In addition, the study proved that the dissipation effect can be expressed by the impulse of the avalanche impact. The impact characteristics against the vertical piles which are arranged to a triangle and the dissipation effect by various types of model dissipators were also discussed.

In the future, the authors will conduct further studies for more effective and economical dissipator types through evaluating the impact on larger scale piles, quantitatively evaluating the closure effect, and examining differences among different snows.

References

1) Yasumasa Itakura and Suteo Tsutsumi: Measurement of Flow Velocity Vector Using a Liquid Crystal Translation Shelf Reticle, Society of Electric Science.
2) Mikio Hino: Spectrum Analysis, Asakura Publishing Co.
3) Yorihiko Oosaki: Introduction to Spectrum Analysis of Seismic Motion, Kajima Publishing Co.
4) Koichi Ogawa, Yasumasa Itakura et al.: Measurement of Mudflow Velocity Using Space Filters, Society of Electric Science.
5) Japanese Association of Mechanization of Construction Works: Handbook of Snow Control Engineering, Morikita Publishing Co.
6) Road Association of Japan: A Report of a Study on Avalanche Control Measures (1), March 1981.
7) Civil Engineering Society: Guidelines for Designing Offshore Steel Structure (Draft), 1973.
8) American Petroleum Institute: Recommended Practice for Planning, Designing and Constructing Fixed Offshore Platform, APL RP 2A, 1981.
9) Architectural Society: Standards for Structural Design of Foundation and Explanatory Notes.
10) Society of Soil Mechanics and Foundation Engineering: Designing Pile Foundation and Explanatory Notes.

Model Test on Avalanche (Part I)
Energy Dissipator

ISSN 0386-5878
Technical Memorandum
No. 2468 July, 1989
Slope Failure Division
Niigata Experimental Laboratory

Key Words: Avalanche, Avalanche Energy Dissipator

Post Card

Postage Stamp

3 0 5 - □ □

Slope Failure Division
Erosion Control Department
Public Works Research Institute
Ministry of Construction
Government of JAPAN
Tsukuba City
Ibaraki, 305, JAPAN

No.

No.

I received copy(ies) of

PWRI technical memorandum No. 2468

M.D.Y.

Name_____